PHYSICAL REVIEW A **93**, 063628 (2016)

Bragg interferometer for gravity gradient measurements

G. D'Amico,[1] F. Borselli,[1] L. Cacciapuoti,[2] M. Prevedelli,[3] G. Rosi,[1] F. Sorrentino,[4] and G. M. Tino[1,*]
[1]*Dipartimento di Fisica e Astronomia and LENS, Università di Firenze, Istituto Nazionale di Fisica Nucleare Sezione di Firenze, via Sansone 1, I-50019 Sesto Fiorentino (FI), Italy*
[2]*European Space Agency, Keplerlaan 1, 2200 AG Noordwijk, The Netherlands*
[3]*Dipartimento di Fisica e Astronomia, Università di Bologna, Via Berti-Pichat 6/2, I-40126 Bologna, Italy*
[4]*Istituto Nazionale di Fisica Nucleare Sezione di Genova, Via Dodecaneso 33, I-16146 Genova, Italy*

(Received 5 April 2016; published 22 June 2016)

We report on the characterization of a dual cloud atom interferometer for gravity gradient measurements using third-order Bragg diffraction as atom optical elements. We study the dependence of the contrast and the gradiometer phase angle against the relevant experimental parameters and characterize the instrument sensitivity. We achieve a sensitivity to gravity gradient measurements of 2.6×10^{-8} s^{-2} (26 E) after 2000 s of integration time.

DOI: 10.1103/PhysRevA.93.063628

I. INTRODUCTION

Light-pulse atom interferometers are extremely sensitive and accurate quantum sensors for the measurement of inertial forces and for testing fundamental physics [1,2].

Nowadays atom interferometry techniques find a vast range of applications especially in metrology and in gravitational physics, where they have been already used for the accurate measurement of gravitational acceleration [3–6], Earth's gravity gradient [7–12] and curvature [13], as gyroscopes [14–17], for tests of the $1/r^2$ law [18] and tests of the Einstein's equivalence principle [19–22], and for the precise measurement of the Newtonian gravitational constant G [9,23–25] and fine-structure constant α [26,27]. The steady improvement in the sensitivity of atom interferometry instruments is opening interesting perspectives for the detection of quantum gravity effects [28] and for the observation of gravitational waves [29–31]. Other important applications are found in geodesy, geophysics, engineering prospecting, and inertial navigation [32,33]. In those cases, particular attention is devoted to the transportability of the apparatus which translates in stringent miniaturization and robustness requirements [34].

Even if the present interferometry instruments already outperform state-of-the-art mechanical and optical devices in the measurement of inertial forces, their sensitivity has not yet reached its ultimate limit. In particular the sensitivity of atom interferometers improves by increasing the momentum transferred to the atoms during the beam splitter and mirror pulses. For this reason, many recent theoretical and experimental efforts [35,36] have been devoted to the development of large momentum transfer (LMT) atom-optics techniques.

One of the most promising LMT techniques consists in the use of Bragg diffraction processes as atom optical elements [37–41]. The interaction between the atomic wave packet and the optical lattice generated by the Bragg lasers allows for a momentum transfer larger than the conventional $2\hbar k$ (k is the wave number of the interacting electromagnetic fields) achieved in two-photon processes (e.g., Raman transitions). In particular, when stimulated on a n-order Bragg process, the atom performs a $2n$-photon transition between two different momentum states separated by $2n\hbar k$. Furthermore, differently from two-photon Raman transitions, Bragg diffraction provides a separation of the interferometric paths only in the external degrees of freedom, while the internal atomic state remains unperturbed. This makes Bragg interferometers less affected by many systematic effects, like ac-Stark and Zeeman shifts.

In this paper we present the first experimental study of the sensitivity and measurement systematics of an atomic gradiometer based on multiphoton Bragg diffraction. Our instrument reaches a sensitivity of 2.6×10^{-8} s^{-2} for gravity gradient measurements. Multiphoton Bragg transitions open interesting perspectives for pushing this sensitivity well beyond the state-of-the-art performance presently achieved with gravity gradiometers based on two-photon Raman processes [8,10].

The paper is organized as follows: Sec. II briefly discusses the theory of atomic Bragg diffraction; in Sec. III we describe the experimental apparatus and the measurement procedure of our Bragg gradiometer; finally, in Sec. IV we present the results of the characterization measurements of our apparatus.

II. BRAGG MATTER-WAVE DIFFRACTION

Bragg diffraction takes place when the atom coherently interacts with a one-dimensional optical lattice generated with two counterpropagating laser beams. For an atomic system, a Bragg diffraction process of order n can be interpreted as a $2n$-photon transition which couples two different momentum states. If the one-dimensional optical lattice is produced by two counterpropagating laser beams, with slightly different frequencies ω_1 and ω_2 and wave numbers $k_1 \simeq k_2$, the complete process consists of the absorption of n photons from one of the laser beams and in the subsequent stimulated emission of n photons in the counterpropagating beam. The transition is then able to transfer a total momentum of $2n\hbar k$ [with $k = (k_1 + k_2)/2$], leaving the atomic internal state unchanged. Figure 1 shows the transition diagram for a third-order Bragg process, connecting the two states $|a,0\rangle \rightarrow |a,6\hbar k\rangle$ in the reference frame where the atom is at rest. After the diffraction,

---

[*] guglielmo.tino@fi.infn.it

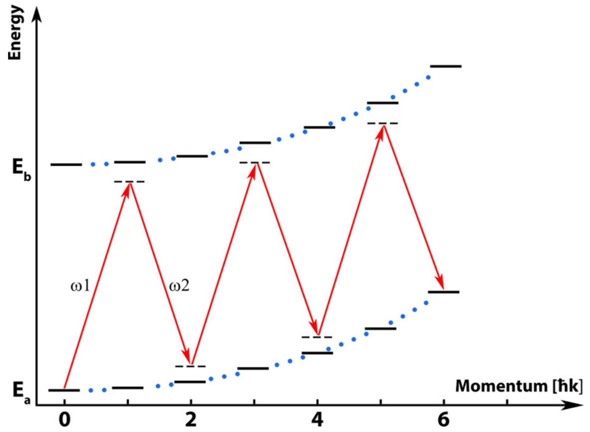

FIG. 1. Schematic representation of a third-order Bragg transition from the state $|a,0\rangle$ to $|a,6\hbar k\rangle$ in the reference frame where the atom is at rest. Here $|a\rangle$ and $|b\rangle$ are two internal atomic states, k is the average wave number of the interacting electromagnetic fields, and ω_1 and ω_2 indicate the frequencies of the two laser beams. The energy in the momentum space follows the parabolic law $n^2\hbar\omega_r$ specified with the dotted blue line.

the atom has acquired a kinetic energy of $(2n\hbar k)^2/(2M) = 4n^2\hbar\omega_r$ [where M is the atomic mass and $\omega_r = \hbar k^2/(2M)$ is the recoil frequency]. This kinetic energy has to balance the energy lost by the laser field, defining the resonance condition for the nth diffraction order as

$$\delta = 4n\omega_r, \tag{1}$$

where $\delta = \omega_1 - \omega_2$.

When the resonance condition in Eq. (1) is met and the duration σ of the Bragg diffraction pulse is $\sigma \gg 1/\omega_r$, atoms are coupled only to the $|2n\hbar k\rangle$ momentum state. This long-interaction-time regime is called the *Bragg regime*. However, as soon as the Bragg pulse duration becomes comparable to $1/\omega_r$, the $|0\rangle$ state can couple to several momentum states (the *quasi-Bragg regime*) and the atomic population is diffracted into different orders [37].

Bragg diffraction from an optical lattice can be described by using the semiclassical treatment extensively discussed in [37]. Considering the scattering of a matter wave from a one-dimensional optical lattice in the reference frame of the lattice ($\delta = 0$) and ignoring all the effects of spontaneous emission, it is possible to demonstrate that the rate equations for the atomic population in the momentum state indexed by m can be written as

$$i\hbar\dot{a}_m = \hbar(\omega_r m^2 + \Omega(t))a_m + \frac{\hbar\Omega(t)}{2}(a_{m+2} + a_{m-2}), \tag{2}$$

where $\Omega(t) = \Omega_0^2(t)/(2\Delta)$ is the two-photon Rabi frequency, Ω_0 is the Rabi frequency, Δ is the single photon detuning, and a_m is the amplitude of the $|m\hbar k\rangle$ momentum state. If we assume as initial conditions $a_{-n} = 1$ and $a_m = 0$ for all $m \neq -n$, for a duration of the Bragg pulse much longer than $1/\omega_r$, the only two momentum states coupled by the interaction are the initial state $-n$ and the state $+n$, which are $2n\hbar k$ apart in momentum space. The solution of the rate equation can thus be written as

$$\begin{aligned} a_{-n}(t) &= \cos\left(\frac{1}{2}\int_{-\infty}^{t}\Omega_{\text{eff}}(t')dt'\right),\\ a_n(t) &= -i\sin\left(\frac{1}{2}\int_{-\infty}^{t}\Omega_{\text{eff}}(t')dt'\right), \end{aligned} \tag{3}$$

where $\Omega_{\text{eff}}(t)$ is defined as

$$\Omega_{\text{eff}} = \frac{\Omega^n}{(8\omega_r)^{n-1}}\frac{1}{[(n-1)!]^2}. \tag{4}$$

Equations (3) and (4) were derived in the Bragg regime where all the intermediate momentum states between $-n$ and n can be neglected. Operation in this regime is therefore completely lossless in the sense that only two momentum states can be coupled by the transition.

In the quasi-Bragg regime, losses in momentum states other than $-n$ and n shall be taken into account. In this case, Eq. (2) leads to a system of coupled differential equations that needs to be solved numerically.

III. EXPERIMENTAL APPARATUS AND PROCEDURE

Our Bragg gravity gradiometer is a dual atom interferometer measuring the differential acceleration between two freely falling clouds of cold ^{87}Rb. The atomic samples are vertically separated by about 30 cm. Figure 2 shows a schematic of the laser system used to induce the Bragg transitions and the main building blocks of the fountain where the atomic samples are in free fall during the interferometric interrogation. For a more complete description of the apparatus see [10,42].

Atoms are initially collected in the vacuum chamber placed at the bottom of the apparatus (not shown in the figure), where a three-dimensional magneto-optical trap (3D-MOT) confines $\sim 10^9$ cold rubidium atoms. The loading rate of the 3D-MOT is enhanced by using a two-dimensional MOT. The sample is then cooled to a temperature of $\sim 4\ \mu$K while being launched vertically inside the interferometric tube with the moving-molasses technique. To have the two freely falling atom clouds needed for the dual interferometer, two atomic clouds are juggled and launched with different velocities to have them simultaneously reaching the apogees of their ballistic trajectories, respectively, at about 60 and 90 cm above the 3D-MOT [43].

After the launch, the atoms enter a magnetically shielded tube in which a uniform magnetic field, oriented along the vertical direction, defines the quantization axis. In our apparatus we are able to probe the atoms on both two-photon Raman and multiphoton Bragg transitions. The first are used during the preparation phase of the atomic sample for the longitudinal velocity selection, while the second are used in the atom interferometry sequence. As shown in Fig. 2, both Raman and Bragg lasers are injected in the same optical fiber, collimated, and circularly polarized before entering the vacuum system. Finally they are retroreflected by a mirror mounted on actuators providing tip-tilt control to compensate for the Coriolis acceleration [44,45]. A linear frequency ramp is applied to both the Raman and Bragg lasers to compensate for the Doppler effect experienced by the freely falling atoms.

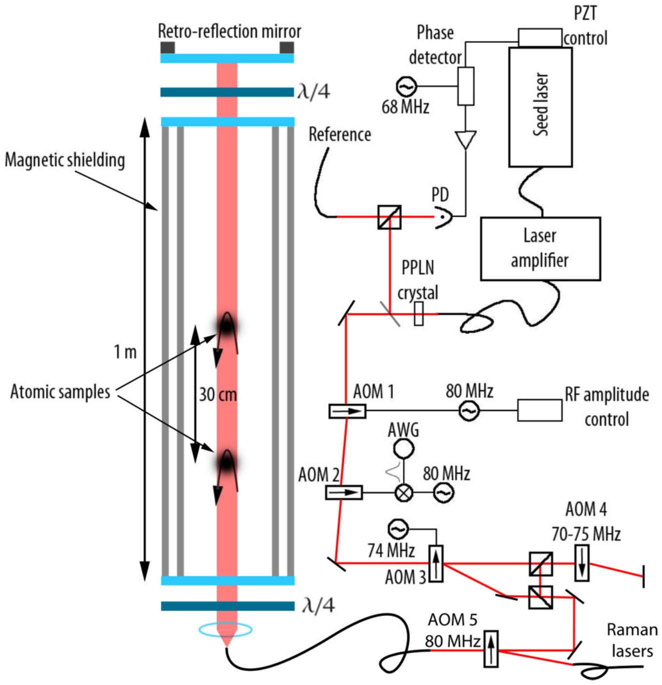

FIG. 2. Schematic representation of the experimental setup. The Bragg beams are derived from a fiber laser system in which the emission of a seed laser is amplified and then frequency doubled. AOM1 is used to stabilize the emission power, AOM2 controls the temporal profile of the interferometric pulses, AOM3 generates the two Bragg beams, and AOM4 steers the frequency difference to account for the Doppler effect during the free fall. The two interferometric beams are then superimposed on the last polarizing beam splitter and injected in a polarization maintaining fiber which delivers the light to the experiment. AOM5 allows us to select whether to switch on the Bragg beams of the interferometer or the Raman beams for the velocity selection.

At the same time this defines the couples of counterpropagating laser beams interacting with the samples.

The atoms are velocity-selected and prepared in the magnetic-field-insensitive $|F=1,m_F=0\rangle$ level of the ground state with a series of three Raman π pulses and three resonant laser pulses which remove atoms in the undesired hyperfine states. This series of pulses prepares $\sim 10^5$ atoms with a narrow vertical velocity distribution of $\sim 0.16 v_r$ full width at half maximum ($v_r = \hbar k/M = 5.8$mm/s is the recoil velocity on the Rb D_2 line). Once the state preparation sequence is completed, the interferometer probes the atoms with a series of three laser pulses which induce the Bragg transitions and act as beam splitters and mirrors for the atomic wave function. The pulses are applied before the atom clouds reach the apogee of their ballistic flight in order to increase the free-fall time before the detection, thus providing a larger spatial separation between the two momentum states representing the two output ports of the interferometer. Our Bragg gradiometer operates at the third difraction order which corresponds to a momentum transfer between the atoms and the light field of $6\hbar k$.

The interferometric sequence is composed of three subsequent Bragg pulses, thus producing a typical Mach-Zehnder interferometer geometry: initially, at $t=0$, a first $\pi/2$ beam-splitting pulse prepares the atomic wave function in an equal and coherent superposition of the two momentum states $|0\rangle$ and $|2n\hbar k\rangle$; after a time T ($T = 80$ ms in our typical working conditions) a mirror π pulse is applied to swap the population in the two momentum states, thus redirecting the atomic trajectories towards the output ports of the interferometer; at $t = 2T$ a last $\pi/2$ pulse is applied to recombine the atomic wave packets.

Since the effective Rabi frequency Ω_{eff} has a strong dependence on the two-photon Rabi frequency Ω [see Eq. (4)], i.e., on laser intensity, in order to drive high-order multiphoton Bragg transitions high-power laser sources are required. In our gradiometer, the Bragg beams are generated by a fiber laser system in which a frequency stabilized seed laser source injects a high-power fiber amplifier. The seed laser (NP Photonics Rock Source) has an emission centered around 1560 nm. This source can be tuned either with a piezo control or with temperature. The light from the seed source injects an Er-doped fiber amplifier (Keopsys fiber amplifier) with a peak emission power of 15 W. The amplified light is then frequency doubled by using two periodically poled lithium niobate crystals and stabilized to the $5S_{1/2}F=2 \rightarrow 5P_{3/2}F'=3$ transition of ^{87}Rb. The detuning from this transition can be controlled and in the typical measurement conditions it is ~ 3 GHz to the blue. Acousto-optical modulators (AOM1, AOM2, and AOM3) stabilize the laser emission power, shape the temporal profile of the interferometric pulses into Gaussian pulses, and split the laser light into the two Bragg beams. Furthermore, since the atoms are in free fall, the resonance condition for the Bragg transition changes at a rate of about 25 MHz/s. This change is compensated by applying a continuous radio-frequency ramp to one of the two Bragg beams by means of AOM4. The light is then injected into a polarization maintaining optical fiber and delivered to the experiment after being collimated to a beam waist of ~ 2 cm. Each Bragg beam has a peak optical power of ~ 500 mW. The injection in the fiber is controlled with AOM5, which allows us to select whether to inject the Raman beams during the velocity selection or the Bragg beams during the interferometric sequence. The polarization of the Bragg beams is modified into circular $\sigma^+ - \sigma^-$ with the use of quarter-wave plates before entering the vacuum apparatus.

At the output of the interferometer, the probability of detecting the atoms in the momentum state $|0\rangle$ is given by $P = (1+\cos\phi)/2$, where ϕ is the phase difference accumulated between the two interferometric arms. In particular, in the presence of a uniform gravity field g, this phase shift can be expressed as $\phi = n(2kgT^2 + \phi_L)$, ϕ_L being the contribution of the Bragg laser phase. A measurement of ϕ is thus equivalent to a measurement of the local acceleration due to the gravitational field along the direction of the imparted momentum $2n\hbar k$. Since ϕ is proportional to the Bragg diffraction order n, the apparatus sensitivity to inertial effects improves as n increases.

In the gradiometer, the two vertically separated atomic clouds are interrogated by the same Bragg lasers, thus realizing two simultaneous gravimeters at different heights. This configuration provides a measurement of the differential acceleration between the two samples through a measurement of the difference in the phase shifts of each interferometer. One of the major advantages of this configuration is its strong

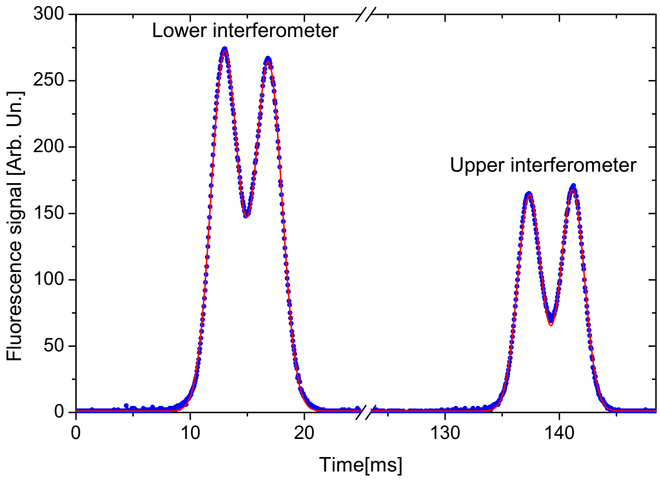

FIG. 3. Typical fluorescence signal obtained at the end of one experimental cycle. The first pair of peaks on the left corresponds to the two interferometric outputs for the lower cloud; the peaks from the upper cloud are on the right. In red we also show a best fit to the data with four Gaussian peaks.

rejection of noise sources, including mechanical vibrations or seismic noise which manifest themselves as common-mode phase noise (ϕ_L) at the two conjugated interferometers.

The entire experimental cycle, which lasts about 2 s, is completed with the measurement of the normalized atomic population in the two different momentum states. Atoms are stimulated by laser light on the cooling transition and detected in time of flight (TOF) by measuring their fluorescence emission. Typical TOF signals are shown in Fig. 3.

Since the Bragg transitions do not change the internal atomic state, differently from a Raman interferometer, the two output ports need to be sufficiently separated in space to be resolved.

After plotting the signal of the upper interferometer versus the lower one, the experimental points distribute along an ellipse. The differential phase shift between the two simultaneous interferometers $\Phi = \phi_u - \phi_l$ (upper and lower interferometers) is proportional to the gravity gradient and it can be obtained from the eccentricity and the rotation angle of the ellipse best fitting the data [46]. We use a least-squares algorithm which fits the parametric equations

$$\begin{cases} x(\theta) = A\sin(\theta) + B \\ y(\theta) = C\sin(\theta + \Phi) + D \end{cases} \qquad 0 \leqslant \theta \leqslant 2\pi$$

to the experimental data, providing the differential phase Φ, which reflects the difference in gravitational acceleration felt by the two vertically displaced interferometers.

IV. CHARACTERIZATION OF THE ATOMIC GRAVITY GRADIOMETER

In this section we characterize our Bragg gradiometer. Section IV A discusses the dependence of the gradiometric contrast with respect to various experimental parameters. In Sec. IV B, we characterize the phase stability of our instrument and its sensitivity to gravity gradient measurements. Section IV C is dedicated to the study of the dependence of the gradiometric signal Φ from different experimental parameters, such as magnetic field, Bragg lasers detuning and optical aperture.

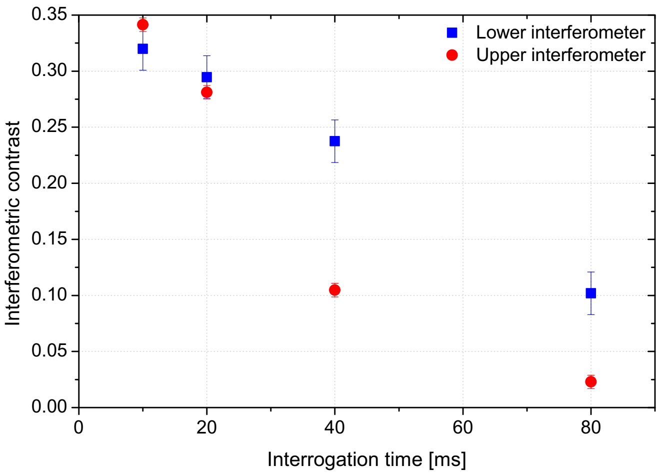

FIG. 4. Interferometer contrast for the upper and lower cloud (in red circles and blue squares, respectively) as a function of the interrogation time T.

A. Gradiometric contrast dependence on significant parameters

1. Dependence of the contrast on the interferometer interrogation time T

We analyzed the dependence of the gradiometric contrast for different interrogation times T. The contrast for the upper and lower interferometers can be obtained from the normalized atomic population interval explored by the ellipse along the vertical and horizontal axes, respectively.

For this characterization, the Bragg pulses had a Gaussian time profile with $\sigma = 24\,\mu$s. Figure 4 shows that the contrast decreases progressively with the increase of the free evolution time T.

One striking characteristic is that the upper atomic cloud loses contrast faster than the lower one with increasing T. This behavior is due to the fact that we launch the two clouds from a single trapping region. Indeed the upper cloud has a 80-ms longer expansion time than the lower cloud before the interferometric sequence. Moreover, the upper sample is also the hotter, due to the heating induced by the light scattered from the lower sample during its loading in the 3D-MOT. As reported in [40], the transition efficiency of the Bragg transitions and consequently also the entire interferometric contrast depend critically on the momentum width and therefore the temperature of the atomic cloud.

In our apparatus, the maximum interferometer duration T is not limited by the loss of contrast, but rather by the need to run the Bragg-pulse sequence entirely during the ascent of the atomic samples to resolve the two interferometric outputs at detection.

2. Dependence of the contrast on the duration of the velocity selection pulses T_{sel}

As described in Sec. III, the longitudinal velocity selection of the sample is realized with the application of three Raman

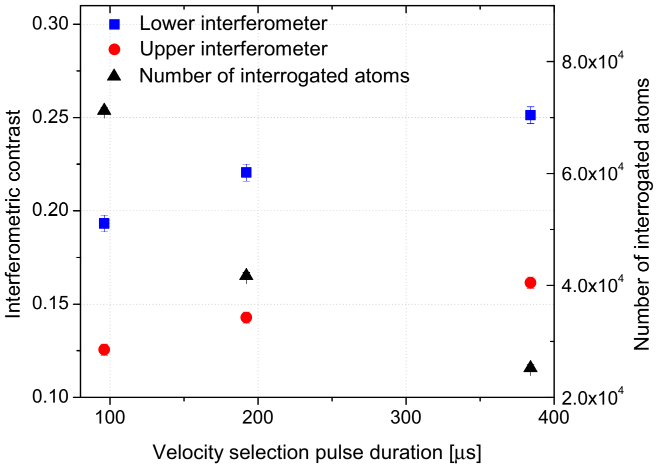

FIG. 5. Interferometer contrast for the upper and lower cloud (in red circles and blue squares, respectively) and number of interrogated atoms (black triangles) as a function of the duration of the Raman velocity selection pulses T_{sel}.

pulses derived from two counterpropagating laser beams. The pulses have a rectangular temporal profile the duration T_{sel} of which determines the selectivity of the process. An increase in the duration T_{sel} translates in a narrower frequency spectrum and thus in a lower number of atoms interacting with the radiation.

For an interrogation time $T = 40$ ms, we measured the contrast for three different durations of the velocity selection pulses. Figure 5 shows an increase in contrast with T_{sel}. This improvement can be attributed to the narrower momentum distribution along the vertical direction obtained when longer selection pulses are applied. Figure 5 also shows the number of atoms at detection as a function of T_{sel}. With the present configuration of our detection scheme [10] the technical noise at detection corresponds to the quantum projection noise (QPN) limit for $\sim$30 000 atoms. Thus for velocity selection pulses shorter than $\sim 200\,\mu$s we can assume that the technical noise is slightly below the QPN limit. For the next measurements we thus fixed the duration of the Raman pulses to $T_{\mathrm{sel}} = 192\,\mu$s. Increasing T_{sel} further would indeed bring only a slight increase in the contrast at the expenses of major losses in terms of detected atoms.

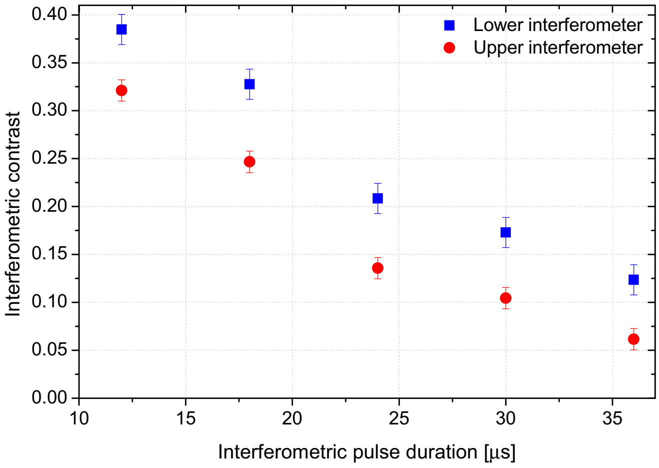

FIG. 6. Interferometer contrast for the upper and lower cloud (in red circles and blue squares, respectively) as a function of the duration of the interferometric pulses σ.

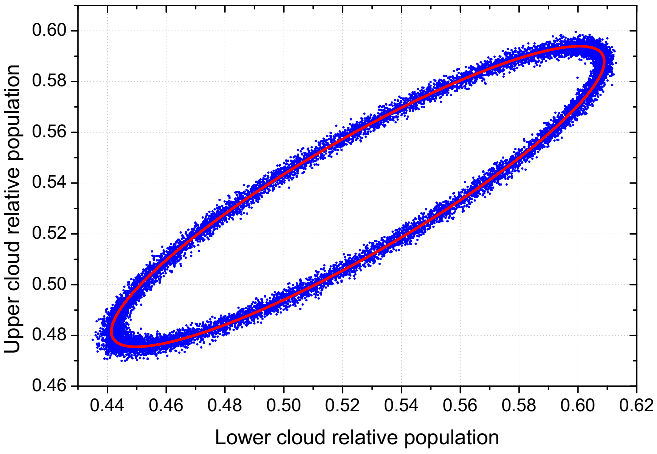

FIG. 7. Ellipse acquired with an interrogation time of $T = 80$ ms and an interferometric pulse duration of $\sigma = 12\,\mu$s. The red continuous curve is the ellipse best fitting the $\sim$14 000 experimental data points.

3. *Dependence of the contrast on the duration of the interferometric pulses σ*

We also studied the interferometer contrast as a function of the temporal width of the Bragg pulses σ which, as discussed in Sec. II, affects the amount of atomic losses in other diffraction orders. With $T = 40$ ms and $T_{\mathrm{sel}} = 192\,\mu$s, we acquired ellipses for five different Bragg pulse durations. Each time we adjust the peak power of the Bragg pulses optimizing the interferometer contrast. Figure 6 shows the contrast as a function of σ. Decreasing the Bragg pulse duration brings a general improvement on the gradiometric contrast. With the present laser system we are technically limited to pulse lengths $\sigma \geqslant 12\,\mu$s due to the optical power available.

However, the contrast improvement obtained for $\sigma = 12\,\mu$s allowed us to operate the interferometer on an interrogation time of $T = 80$ ms, thus quadrupling the instrument sensitivity to accelerations. An example of the gradiometric ellipses obtained in these conditions is shown in Fig. 7 together with a least-squares fit of the experimental data.

As mentioned in Sec. II, operation in the ideal Bragg regime requires that the temporal duration of the Bragg pulses σ is $\sigma \gg 1/\omega_r$. Our instrument is presently operated in the quasi-Bragg regime since $1/\omega_r \simeq 42\,\mu$s.

B. Phase stability and sensitivity

To evaluate the phase stability and sensitivity of our apparatus, we calculated the Allan deviation of the gradiometric phase angle over an integration time of about 8 h. The Allan deviation (see Fig. 8) decreases as $1/\sqrt{t}$ (t is the integration time expressed in seconds), showing that our gradiometer is mainly affected by white phase noise. Due to the large error bars at large times we can exclude the presence of a flicker floor only up to 1000 s of integration time.

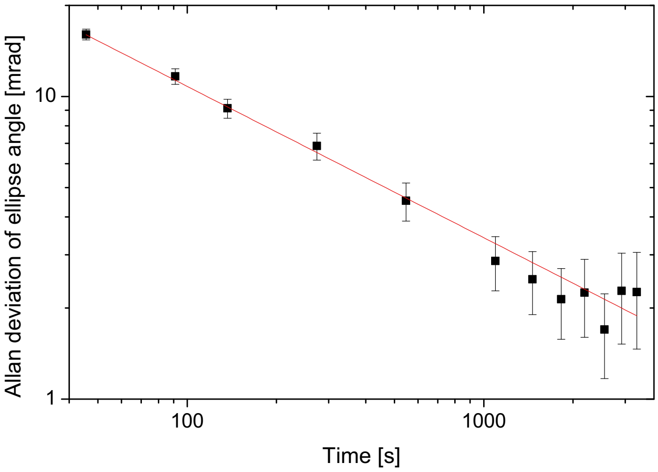

FIG. 8. Allan deviation of the differential phase angle extracted from the ellipse fitting of the gravity gradiometer data. The fit to the Allan deviation data with the function $\sigma_\Phi = a/\sqrt{t}$, where t is the integration time in seconds, is shown in red.

After fitting the Allan deviation data (red curve), we evaluate the short and long term sensitivities of our apparatus to gravity gradients and differential accelerations. Considering the vertical displacement of 30 cm of our atomic samples, the instrument sensitivity to gravity gradient measurements is 1.2×10^{-6} s^{-2} at 1 s of integration time, down to 2.6×10^{-8} s^{-2} at 2000 s, corresponding to a sensitivity for differential accelerations of $3.6 \times 10^{-8} g$ at 1 s, down to $8.0 \times 10^{-10} g$ after 2000 s.

C. Gradiometric signal dependence on significant parameters

In this section we analyze the dependence of the gradiometric signal Φ from the relevant experimental parameters.

In general, we can decompose the gradiometric signal as the sum of a part which depends on odd powers of k, Φ_o (e.g., signal from the gravity gradient and residual Coriolis acceleration), and a part which depends on even powers of k, Φ_e (e.g., one-photon light shift), i.e., $\Phi = \Phi_o + \Phi_e$. To reject all the systematic errors which induce phase shifts depending on even powers of k we use the k-reversal technique [47]. We reverse the direction of the momentum transferred to the atoms at each experimental cycle, obtaining two different ellipses corresponding to the two opposite directions of the k vector (see Fig. 9). From each of the two ellipses we can thus derive the angle $\Phi_{\mathrm{dir,rev}}$. The combination

$$\Phi_o = \frac{\Phi_{\mathrm{dir}} - \Phi_{\mathrm{rev}}}{2} \tag{5}$$

efficiently rejects all systematic effects which depends on even powers of k. All our measurements apply this procedure.

1. *Gradiometric signal dependence on the magnetic quantization field*

As mentioned in Sec. III, a uniform magnetic field oriented along the 1-m-long vertical tube of the interferometer defines the quantization axis for the atoms. Furthermore the region inside the tube is shielded from external magnetic fields by two μ-metal layers.

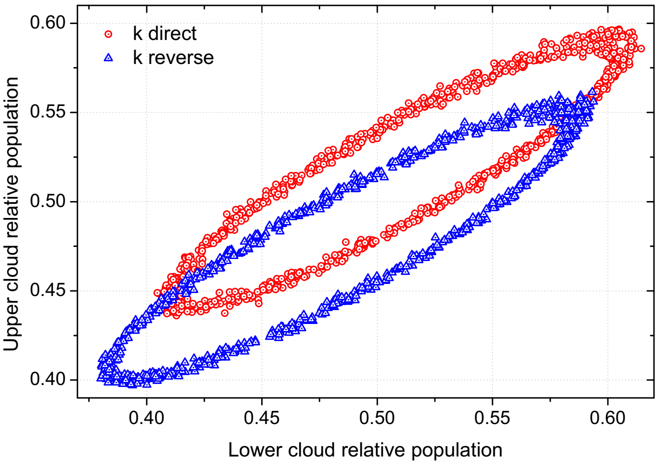

FIG. 9. Gradiometric ellipses acquired with the k-reversal procedure. Combining the angles derived from each single ellipse, Φ_{dir} and Φ_{rev}, it is possible to cancel the phase contributions dependent on even powers of k.

To evaluate the systematic effect produced by uncontrolled magnetic fields in the interferometric region, we measured the differential phase of the gravity gradiometer [see Eq. (5)] for six different values of the current in the bias field solenoid. For each of these values we calculated the angle Φ_o using Eq. (5).

The effects of the magnetic field on the interferometric signal can be evaluated by introducing in the Lagrangian the term for the quadratic Zeeman effect:

$$\mathcal{L}_B(x,\dot{x}) = 2\pi\hbar\beta B^2(x), \tag{6}$$

with $\beta = 28.8\,\mathrm{GHz/T^2}$. Inside the interferometric tube we can suppose to have a magnetic field which over the extent of the atomic clouds trajectories can be expressed as

$$B(x) = B_0 + B'x, \tag{7}$$

where B_0 and B' represent the magnetic field bias and gradient produced by both the solenoid surrounding the interferometer tube and by any other field source. Substituting in Eq. (6), we obtain

$$\begin{aligned}\mathcal{L}(x,\dot{x}) &= 2\pi\hbar\beta\left(B_0^2 + 2B_0B'x + B'^2x^2\right)\\ &= K + Ma_mx + M\frac{\gamma_m}{2}x^2,\end{aligned} \tag{8}$$

with $a_m = 4\pi\frac{\hbar}{M}\beta B_0 B'$ and $\gamma_m = 4\pi\frac{\hbar}{M}\beta B'^2$.

A magnetic field with a linear gradient determines a Lagrangian equivalent to that of a uniform gravitational field plus a linear gradient. The corresponding phase shift for the single interferometer is then given by [48]

$$\phi_m = 2nk\left[a_mT^2 + \frac{\gamma_m T^3}{12}\left(12v_0 + 6v_r - 7a_mT\right) + O\left(\gamma_m^2\right)\right]. \tag{9}$$

This term will not be canceled by the k-reversal procedure and from Eq. (9) we can evaluate the systematic shift which affects the gradiometric measurement. Labeling with u and l the magnetic field bias and gradient experienced by the upper and lower clouds we obtain

$$\Phi_m = \alpha\left[B_0^u B'^u - B_0^l B'^l\right], \tag{10}$$

with $\alpha = 4\pi \frac{2n\hbar k}{M}\beta T^2 \simeq 82 \times 10^6 \frac{\text{rad m}}{\text{T}^2}$.

As B_0 and B' carry the contributions of both the field generated by the solenoid and residual magnetic fields, we expect a quadratic dependence of Φ_o from the current injected in the solenoid:

$$\Phi_o = \Phi_{I^2} + \Phi_I + C. \tag{11}$$

If we indicate with B_I and B_R the field generated by the solenoid and the residual fields experienced by the atoms, the I^2 term in Eq. (11) will contain the contributions of B_I and B'_I, the I term will contain the mixed products $B_I \cdot B'_R$ and $B_R \cdot B'_I$, while the last term will contain the contributions of B_R and B'_R.

The gradiometric phase angle as a function of the solenoid current is reported in Fig. 10 together with a second-order polynomial fit of the experimental data, $\Phi_o = aI^2 + bI + C$. From the fit we can extrapolate the single contributions of Eq. (11):

$$C = (426.7 \pm 1.2)\ \text{mrad},$$
$$b = (7.9 \pm 2.2) \times 10^{-2}\ \text{mrad/mA},$$
$$a = (-1.1 \pm 0.1) \times 10^{-2}\ \text{mrad/mA}^2.$$

Considering that $B_I = 1.1\ \mu\text{T/mA}$ in our apparatus, it is possible to estimate $B'_I = |a|/(\alpha B_I) = 0.1\ \mu\text{T/(m mA)}$. If we now suppose that the linear term is dominated by the residual magnetic gradient B'_R, we can also derive an upper limit for this parameter:

$$B'_R < \frac{b}{\alpha B_I} = 0.88 \frac{\mu\text{T}}{\text{m}}. \tag{12}$$

The same reasoning can also be applied to obtain an upper limit for B_R:

$$B_R < \frac{b}{\alpha B'_I} = 7.9\ \mu\text{T}. \tag{13}$$

We can now establish an upper limit for the systematic shift introduced by the residual magnetic fields:

$$\Phi_m^R < \alpha B_R B'_R = \frac{b^2}{a} \simeq (0.6 \pm 0.4)\ \text{mrad}. \tag{14}$$

Since the lower atomic sample is near the entrance of the tube when the interferometric sequence is applied, i.e., in a region where the magnetic shielding is less effective and where the produced magnetic field is not so well characterized, we can assume that a large fraction of this systematic shift comes from the lower interferometer.

2. *Gradiometric signal dependence on the detuning*

In order to evaluate the dependence of the gradiometric signal on the frequency detuning of the Bragg beams, we acquired ellipses by varying the detuning in 50-MHz steps around a blue detuning of ≃3.269 GHz, representing our standard working condition. The results are shown in Fig. 11.

By varying the detuning of the Bragg lasers, we expect to change the amount of the atomic losses towards diffraction orders other than $n = 3$. Since these loss mechanisms affect in the same way both the upper and lower interferometers of the gradiometer, we expect a strong rejection of any related shift. The measurements in Fig. 11 are all compatible within our experimental error. At this level we cannot thus detect any effect of the detuning on the gradiometric signal.

3. *Gradiometric signal dependence on the optical aperture*

The two Bragg beams are delivered to the experiment through a common polarization-maintaining optical fiber. The fiber output is collimated into a Gaussian beam with a waist of about 2 cm. A more uniform illumination of the atomic clouds results in an improved gradiometric contrast. In contrast, large

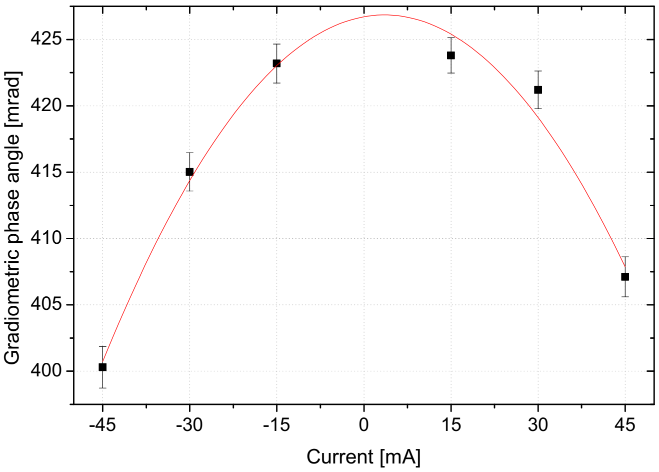

FIG. 10. Gradiometric phase angle Φ for different values of the current in the bias solenoid. In red is shown a second-order polynomial fit of the data.

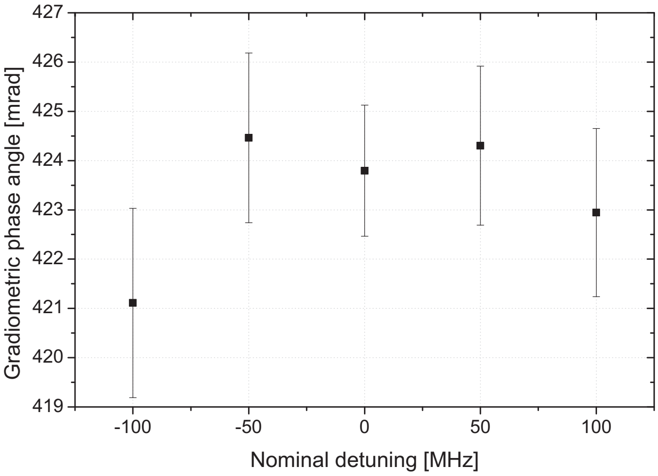

FIG. 11. Gradiometric signal dependence on the detuning of the Bragg beams. The applied detuning is measured with respect to our standard detuning working condition, i.e., ≃3.269 GHz to the blue of the ^{87}Rb D_2 line.

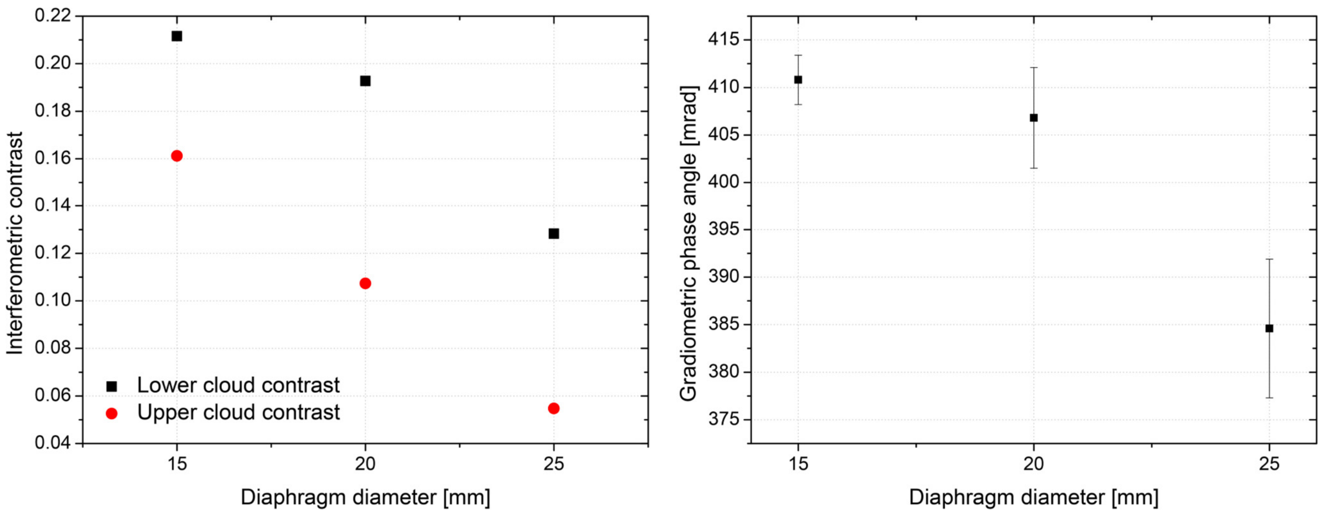

FIG. 12. (Left) Dependence of the interferometer contrast with the diaphragm aperture for both the upper and lower atomic clouds (red circles and black squares, respectively). (Right) Gradiometric phase angle measured for the three different apertures.

Bragg beams have two obvious disadvantages: they require more power to interrogate the atoms; moreover, they produce diffraction effects through the finite-size apertures of the optics used for the beam shaping and ultimately from the windows of the interferometer tube. We have placed a diaphragm right after the collimating lens and varied its aperture to be able to modify the intensity profile which illuminates the atomic clouds both in the transverse and longitudinal directions and to study diffraction-induced effects on the gravity gradiometer phase. An extensive treatment of the diffraction problem of a Gaussian beam from a circular aperture can be found in [49].

In this configuration, we acquired ellipses for three different diaphragm diameters, respectively, 25, 20, and 15 mm. With our present optical configuration we cannot decrease further the aperture of the diaphragm without blocking the laser beams needed during the sample preparation sequence to eliminate atoms in undesired hyperfine states, as mentioned in Sec. III. The results for the interferometric contrasts and ellipse phase angle are reported in Fig. 12.

The contrast of both the upper and lower interferometer has a strong dependence on the diaphragm aperture and shows a rapid decrease, with slightly different trends between the upper and lower interferometer, when the aperture diameter is increased. Since the detection beam has a transverse extension of 15 mm we can safely assume that the observed effects are not due to the decreased number of atoms interrogated when the optical aperture diameter is reduced. Even if a quantitative analysis of these diffraction effects is beyond the scope of this work, we can suppose that the observed loss of contrast and the influence on the gradiometric signal are introduced by the variations of the beam intensity profile, which are due to diffraction from the optical aperture that strongly affects both the longitudinal and transverse intensity profiles. The irregularity in the longitudinal profile in particular brings different ac-Stark shifts for the vertically separated atomic clouds, which cannot be rejected in the differential measurement scheme of the gradiometer.

For what concerns the contrast a qualitative understanding of the results shown can be found considering Eq. (28) in [49]. The equation expresses the light intensity along the propagation axis for a Gaussian laser beam, after traversing a circular aperture. Considering the derivative of this quantity with respect to the distance from the circular aperture [we can neglect the term $(z/d)^2$ in our experimental conditions, where z is the distance from the optical aperture and d is the Rayleigh range], we obtain a function which has a maximum when the aperture radius equals the waist of the Gaussian beam. In our system the radius of the vacuum tube is 17.5 mm, thus the limiting optical aperture is the diaphragm aperture radius. Since our beam has a waist of ~20 mm, reducing the diaphragm aperture radius would result in a decreased intensity gradient along the propagation axis which translates in the observed increase of contrast.

V. CONCLUSIONS

We reported on the design and characterization of a third-order Bragg gravity gradiometer. Our measurements characterize the dependence of the interferometric contrast and gradiometric signal as a function of the relevant experimental parameters.

We also evaluated the sensitivity of our instrument. In the present conditions, we can reach a sensitivity to gravity gradients of $1.2 \times 10^{-6}\ \mathrm{s}^{-2}$ after 1 s of integration, down to $2.6 \times 10^{-8}\ \mathrm{s}^{-2}$ (26 E) after 2000 s. In the future, we expect to improve the instrument performance by optimizing the intensity profile of the Bragg lasers, which is presently our major source of systematic error. In addition, we are working towards the implementation of colder atomic sources to reduce the transverse momentum spread of the samples.

ACKNOWLEDGMENTS

This work was supported by Istituto Nazionale di Fisica Nucleare (MAGIA-Advanced experiment) and Ministero dell'Istruzione, dell'Università e della Ricerca (Atom Interferometry project).

[1] A. D. Cronin, J. Schmiedmayer, and D. E. Pritchard, Rev. Mod. Phys. **81**, 1051 (2009).

[2] *Atom Interferometry, Proceedings of the International School of Physics Enrico Fermi, Course CLXXXVIII*, edited by G. M. Tino and M. A. Kasevich (Società Italiana di Fisica and IOS Press, Amsterdam, 2014).

[3] M. Kasevich and S. Chu, Appl. Phys. B **54**, 321 (1992).

[4] A. Peters, K. Y. Chung, and S. Chu, Nature (London) **400**, 849 (1999).

[5] H. Müller, S. W. Chiow, S. Herrmann, S. Chu, and K. Y. Chung, Phys. Rev. Lett. **100**, 031101 (2008).

[6] J. L. Gouët, T. Mehlstäubler, J. Kim, S. Merlet, A. Clairon, A. Landragin, and F. P. DosSantos, Appl. Phys. B **92**, 133 (2008).

[7] M. J. Snadden, J. M. McGuirk, P. Bouyer, K. G. Haritos, and M. A. Kasevich, Phys. Rev. Lett. **81**, 971 (1998).

[8] J. M. McGuirk, G. T. Foster, J. B. Fixler, M. J. Snadden, and M. A. Kasevich, Phys. Rev. A **65**, 033608 (2002).

[9] A. Bertoldi, G. Lamporesi, L. Cacciapuoti, M. de Angelis, M. Fattori, T. Petelski, A. Peters, M. Prevedelli, J. Stuhler, and G. M. Tino, Eur. Phys. J. D **40**, 271 (2006).

[10] F. Sorrentino, Q. Bodart, L. Cacciapuoti, Y. H. Lien, M. Prevedelli, G. Rosi, L. Salvi, and G. M. Tino, Phys. Rev. A **89**, 023607 (2014).

[11] F. P. DosSantos, Phys. Rev. A **91**, 063615 (2015).

[12] Y. P. Wang, J. Q. Zhong, X. Chen, R. B. Li, D. W. Li, L. Zhu, H. W. Song, J. Wang, and M. S. Zhan, Opt. Commun. **375**, 34 (2016).

[13] G. Rosi, L. Cacciapuoti, F. Sorrentino, M. Menchetti, M. Prevedelli, and G. M. Tino, Phys. Rev. Lett. **114**, 013001 (2015).

[14] T. L. Gustavson, P. Bouyer, and M. A. Kasevich, Phys. Rev. Lett. **78**, 2046 (1997).

[15] T. L. Gustavson, A. Landragin, and M. A. Kasevich, Class. Quantum Grav. **17**, 2385 (2000).

[16] B. Canuel, F. Leduc, D. Holleville, A. Gauguet, J. Fils, A. Virdis, A. Clairon, N. Dimarcq, C. J. Bordé, A. Landragin, and P. Bouyer, Phys. Rev. Lett. **97**, 010402 (2006).

[17] A. Gauguet, B. Canuel, T. Lévèque, W. Chaibi, and A. Landragin, Phys. Rev. A **80**, 063604 (2009).

[18] G. Ferrari, N. Poli, F. Sorrentino, and G. M. Tino, Phys. Rev. Lett. **97**, 060402 (2006).

[19] S. Fray, C. A. Diez, T. W. Hänsch, and M. Weitz, Phys. Rev. Lett. **93**, 240404 (2004).

[20] S. Dimopoulos, P. W. Graham, J. M. Hogan, M. A. Kasevich, and S. Rajendran, Phys. Rev. D **78**, 122002 (2008).

[21] M. G. Tarallo, T. Mazzoni, N. Poli, D. V. Sutyrin, X. Zhang, and G. M. Tino, Phys. Rev. Lett. **113**, 023005 (2014).

[22] L. Zhou, S. Long, B. Tang, X. Chen, F. Gao, W. Peng, W. Duan, J. Zhong, Z. Xiong, J. Wang, Y. Zhang, and M. Zhan, Phys. Rev. Lett. **115**, 013004 (2015).

[23] J. B. Fixler, G. T. Foster, J. M. McGuirk, and M. A. Kasevich, Science **315**, 74 (2007).

[24] G. Lamporesi, A. Bertoldi, L. Cacciapuoti, M. Prevedelli, and G. M. Tino, Phys. Rev. Lett. **100**, 050801 (2008).

[25] G. Rosi, F. Sorrentino, L. Cacciapuoti, M. Prevedelli, and G. M. Tino, Nature (London) **510**, 518 (2014).

[26] A. Wicht, J. M. Hensley, E. Sarajilic, and S. Chu, Phys. Scr. **T102**, 82 (2002).

[27] M. Cadoret, E. de Mirandes, P. Cladé, S. Guellati-Khélifa, C. Schwob, F. Nez, L. Julien, and F. Biraben, Phys. Rev. Lett. **101**, 230801 (2008).

[28] G. Amelino-Camelia, C. Lämmerzahl, F. Mercati, and G. M. Tino, Phys. Rev. Lett. **103**, 171302 (2009).

[29] G. M. Tino and F. Vetrano, Class. Quantum Grav. **24**, 2167 (2007).

[30] S. Dimopoulos, P. W. Graham, J. M. Hogan, M. A. Kasevich, and S. Rajendran, Phys. Lett. B **678**, 37 (2009).

[31] G. M. Tino, F. Vetrano, and C. Lämmerzahl, Gen. Relativ. Gravit. **43**, 1901 (2011).

[32] A. Bresson, Y. Bidel, P. Bouyer, B. Leone, E. Murphy, and P. Silvestrin, Appl. Phys. B **84**, 545 (2006).

[33] M. de Angelis, A. Bertoldi, L. Cacciapuoti, A. Giorgini, G. Lamporesi, M. Prevedelli, G. Saccorotti, F. Sorrentino, and G. M. Tino, Meas. Sci. Technol. **20**, 022001 (2009).

[34] M. Hauth, C. Freier, V. Schkolnik, A. Senger, M. Schmidt, and A. Peters, Appl. Phys. B **113**, 49 (2013).

[35] H. Müller, S. W. Chiow, S. Herrmann, and S. Chu, Phys. Rev. Lett. **102**, 240403 (2009).

[36] S. W. Chiow, T. Kovachy, H. C. Chien, and M. A. Kasevich, Phys. Rev. Lett. **107**, 130403 (2011).

[37] H. Müller, S. W. Chiow, and S. Chu, Phys. Rev. A **77**, 023609 (2008).

[38] D. M. Giltner, R. W. McGowan, and S. A. Lee, Phys. Rev. A **52**, 3966 (1995).

[39] H. Müller, S. W. Chiow, Q. Long, S. Herrmann, and S. Chu, Phys. Rev. Lett. **100**, 180405 (2008).

[40] S. S. Szigeti, J. E. Debs, J. J. Hope, N. P. Robins, and J. D. Close, New J. Phys. **14**, 023009 (2012).

[41] P. A. Altin, M. T. Johnsson, V. Negnevitsky, G. R. Dennis, R. P. Anderson, J. E. Debs, S. S. Szigeti, K. S. Hardman, S. Bennetts, G. D. McDonald, L. D. Turner, J. D. Close, and N. P. Robins, New J. Phys. **15**, 023009 (2013).

[42] M. Prevedelli, L. Cacciapuoti, G. Rosi, F. Sorrentino, and G. M. Tino, Phil. Trans. R. Soc. A **372**, 2026 (2014).

[43] R. Legere and K. Gibble, Phys. Rev. Lett. **81**, 5780 (1998).

[44] J. M. Hogan, D. M. S. Johnson, and M. A. Kasevich, in *Proceedings of the International School of Physics Enrico Fermi, Course CLXVIII on Atom Optics and Space Physics*, edited by E. Arimondo, W. Ertmer, W. P. Schleich, and E. M. Rasel (IOS, Oxford, 2007), p. 411.

[45] S. Y. Lan, P. C. Kuan, B. Estey, P. Haslinger, and H. Müller, Phys. Rev. Lett. **108**, 090402 (2012).

[46] G. T. Foster, J. B. Fixler, J. M. McGuirk, and M. A. Kasevich, Opt. Lett. **27**, 951 (2002).

[47] A. Louchet-Chauvet, T. Farah, Q. Bodart, A. Clairon, A. Landragin, S. Merlet, and F. Pereira Dos Santos, New J. Phys. **13**, 065025 (2011).

[48] A. Peters, K. Y. Chung, and S. Chu, Metrologia **38**, 25 (2001).

[49] R. G. Schell and G. Tyras, J. Opt. Soc. Am. **61**, 31 (1971).